The Astrophysical Journal, 769:60 (13pp), 2013 May 20 doi:10.1088/0004-637X/769/1/60

EFFECT OF COULOMB COLLISIONS ON THE GRAVITATIONAL SETTLING OF LOW AND HIGH FIRST IONIZATION POTENTIAL ELEMENTS

Iselin M. Th. Bø[1], Ruth Esser[2], and Øystein Lie-Svendsen[3]
[1] Piazza Europa 16, I-52026 Pian di Scò (AR), Italy; iselinbo@online.no
[2] Institute of Science and Technology, University of Tromsø, NO–9037 Tromsø, Norway; ruth.esser@uit.no
[3] Norwegian Defence Research Establishment (FFI), P.O. Box 25, NO–2027 Kjeller, Norway; Oystein.Lie-Svendsen@ffi.no
Received 2012 December 4; accepted 2013 April 4; published 2013 May 6

ABSTRACT

We model the effect of gravitational settling in the upper chromosphere on O, Fe, Si, and Ne, studying whether Coulomb collisions between ionized low First Ionization Potential (FIP) elements and protons is sufficient to cause abundance enhancements relative to oxygen. We find that low-FIP abundance enhancements comparable to observed values can be obtained provided the hydrogen ionization degree lies in the approximate range 10%–30%, which agrees with chromospheric models. Lower or higher hydrogen ionization causes the FIP-effect to become smaller or absent (depletion of all heavy elements). Iron must be almost fully ionized in order to become enriched relative to high-FIP elements, and this requires a high iron photoionization rate. The time scale necessary to produce the enrichment increases rapidly with increasing H ionization. For iron in a background from a semiempirical chromospheric model, with an H ion fraction of the order of 30%–40% in the upper chromosphere, 1–2 hr of settling is required to produce enhancements comparable to observations. The absolute abundance (relative to H), which monotonically decreases with time during settling, has by that time decreased by less than 50% in the same altitude region. With the same background conditions, the silicon abundance is more strongly enhanced by the settling than the iron abundance. The high-FIP element neon is depleted, relative to O and low-FIP elements, in the same background and altitude region where iron is enhanced, typically by 50% or more relative to O after 1–2 hr of settling.

Key words: Sun: abundances – Sun: chromosphere – Sun: corona

Online-only material: color figures

1. INTRODUCTION

Measurements of the composition of the upper solar atmosphere carried out over several decades reveal systematic differences between the elemental composition of the photosphere and corona (e.g., Feldman & Widing 2003). The enhancement of elements with low First Ionization Potential (FIP) relative to high-FIP elements depends on the structure in which they are observed. In the fast solar wind, for example, the observed abundances are close to photospheric values with only very small enhancements of low-FIP relative to high-FIP elements (Gloeckler & Geiss 2007). In streamer regions on the other hand, Solar Ultraviolet Measurement of Emitted Radiation observations close to the solar surface show high-FIP elemental abundances close to photospheric and low-FIP elements enhanced by a factor of four (Feldman et al. 1998). In addition, absolute abundance enhancements of low FIP-elements have been reported by several authors (e.g., White et al. 2000; Raymond et al. 1997). Investigations of a large number of different coronal structures led to the conclusion that the FIP fractionation strongly depends on plasma structures (Dwivedi et al. 1999) and might also vary in time (e.g., Feldman & Widing 2003).

It is commonly assumed that this FIP fractionation originates in the chromosphere. In closed field regions, an additional depletion of all heavy elements might occur at larger heights in the corona with heavier elements falling off faster than the lighter ones. This effect can be explained with gravitational settling (Raymond 1999). A large number of theoretical models have been developed to determine the physical processes that lead to the FIP effect in the chromosphere. A review of suggested mechanisms leading to FIP dependent abundance variations can be found in Hénoux (1998). That review includes models where the magnetic field plays an active role (e.g., Vauclair 1996) and models where the magnetic field, if present at all, only specifies the flow direction of the ions (e.g., Wang 1996).

In the chromosphere, mechanisms have to exist that counteract gravitational settling which would fractionate according to mass not FIP. The mechanism(s) counteracting the gravitational pull on the elements in the chromosphere might not be the same in different chromospheric regions underlying the various coronal structures. It was shown, for example, that in the chromospheric source region of the fast solar wind, the frictional drag by fast flowing hydrogen on the heavy elements might be sufficient to get the ions to the top of the chromosphere (Pucci et al. 2010). In regions underlying coronal loops, there is no net outflow of hydrogen and gravitational settling will lead to a large reduction of the heavy element abundance unless some other process keeps the chromosphere well mixed. Above the temperature minimum, the chromosphere is convectively stable and the mixing process will have to be done by some external process such as reconnection or strong and sudden heating.

It was shown (Killie & Lie-Svendsen 2007) that if the mixing happens too often high FIP-elements will leak into the corona, whereas low FIP-elements are unable to pass through the region where hydrogen becomes ionized because of the down-streaming of the protons in that region. Too frequent mixing can thus lead to a reverse FIP-effect. On the other hand, the mixing cannot happen too rarely since the heavy elements may settle completely.

Laming (2004) investigated the effect of the ponderomotive force of Alfvén waves in regions underlying closed field coronal loops. Gravitational settling was inhibited by imposing a flow on

the background hydrogen (equivalent to very frequent mixing events). In the present paper, we also focus on the closed field regions, but we shall allow for gravitational settling between mixing events and we investigate the role that Coulomb collisions play in counteracting the gravitational settling of the ions in an atmosphere that is well mixed to start with. Since the settling depends on the chromospheric degree of ionization, we shall consider both a "realistic" background chromosphere, from the model by Fontenla et al. (1990), and models with varying hydrogen ionization, obtained by varying the H photoionization rate.

The model that is used to calculate the gravitational settling of O, Si, Ne, and Fe takes into account ionization processes, pressure gradient, gravity, the electric field generated by the electrons and collisions between heavy elements and hydrogen. Heavy elements move downward faster than hydrogen due to the gravitational pull. At upper-chromospheric temperatures, low FIP-elements have a high ionization degree relative to high FIP-elements and may experience a much stronger Coulomb force from the protons even for a low hydrogen ionization (because the Coulomb cross section is much larger than the neutral–neutral and neutral–ion cross sections). The question is whether the Coulomb interaction with the protons might under certain circumstances delay the gravitational settling of the low FIP-elements enough to create an enhancement of these elements relative to the high FIP-elements that is of the same order as observed in the low corona.

The model investigates what happens to the gas from the time right after it has been mixed by some mechanism, such as reconnection or sudden heating. The changing composition is followed in time. The effect of the gravitational settling is strong, however; in order for the Coulomb interaction to produce the observed abundances, a mechanism has to exist that regularly removes the gas from the top of the chromosphere. This could be achieved by reconnection or some other form of strong heating (e.g., wave energy dissipation). The process where the Coulomb forces counteract the gravitational pull on the ions is thus limited not only by the time scale of the gravitational settling but also by the time scales of the "outer" processes, namely mixing and removal from the top. These outer processes are not included in our model.

The fractionation of an element must be determined by three parameters: the atomic mass of the element, the ionization degree, and, possibly, the "size" of the element which enters in the cross section for collisions with the hydrogen background. Fractionation by mass would make the light elements overabundant compared with heavier elements, which is not observed. We therefore focus on the effect of the ionization degree, the premise being that low-FIP elements (lower FIP than hydrogen) are ionized before hydrogen, while high-FIP elements are ionized after hydrogen. In addition, there will be some effect from the atomic size, which is included in our model. For instance, neon has an atomic polarizability that is less than 1/20 of the iron polarizability, implying that the cross section for collisions between neutral iron and protons is more than four times the cross section for neon-proton collisions, which in itself can lead to an enhancement in the iron abundance relative to the neon abundance.

2. THE MODEL

The region of the solar atmosphere that will be modeled in the following covers approximately the uppermost 300 km of the chromosphere, up to the chromosphere/transition region interface, and is sketched in Figure 1. Below the upper chromosphere, gravitational settling timescales can be of the order of months such that even a very infrequent mixing process will keep abundances close to photospheric values in the region where the lower boundary of the model is placed. The transition region forms a natural upper boundary because of the strong thermal force that acts on minor ions in the transition region (Nakada 1969). This force pulls heavy ions up the temperature gradient into the corona, even in cases of moderate proton downflow, and basically prevents minor (heavy) ions from entering the lower transition region and chromosphere from the corona (Killie & Lie-Svendsen 2007), except in cases of very strong proton downflow (which requires that the downward heat conduction from the corona is suddenly switched off). The thermal force does not apply to neutral particles. However, even high-FIP elements will become ionized in the transition region. By putting the upper boundary at (or close to) the chromosphere-transition region interface, we shall therefore assume that during the gravitational settling no minor particles, ionized or neutral, enter the modeled slab through the upper boundary. If we had put the boundary below this interface, then this boundary condition would not be appropriate as settling would then also have affected the region above the upper boundary of the model.

By limiting ourselves to the upper chromosphere, we shall only solve the continuity and momentum equation for the neutral and singly ionized species. We do not include an energy equation, but instead assume a given temperature profile (that would have been determined by the balance between chromospheric heating and radiative losses). The temperature, assumed equal for all species, extends from $T_e \approx 7000$ K at the lower boundary up to $T_e = 10^4$ K at the transition region interface, and we choose two (quite similar) temperature profiles, a linear profile and a nonlinear profile obtained from Model 1 of Fontenla et al. (1990), henceforth referred to as "FAL 1." The latter is identical to model C of Vernazza et al. (1981) below approximately 8000 K. The profiles are shown in Figure 2.

The minor species are treated as test particles in a given steady-state hydrogen background. Hence, the H background does not change during the gravitational settling. Helium, which is not a minor element, is not included. We shall use five different H background solutions. In Section 3, the background is taken from the FAL 1 model of Fontenla et al. (1990). In Section 4, it is obtained by integrating the continuity and momentum equations for neutral hydrogen and protons until a steady state is reached, for four different values of the H photoionization rate, leading to four different ionization profiles.

We assume horizontal homogeneity and flow only in the vertical direction z. For each particle specie i we solve the time-dependent continuity and momentum equations. The continuity equation reads

$$\frac{\partial n_i}{\partial t} + \frac{\partial (n_i u_i)}{\partial z} = n_j P_{ji} - n_i P_{ij}, \quad (1)$$

where t denotes time, n_i and u_i are the density and flow speed of particle specie i, and P_{ij} is the transition rate from specie i to specie j caused by ionization or recombination. For ionization we use the direct rates of Arnaud & Rothenflug (1985), except for iron (Fe), which we take from Arnaud & Raymond (1992). Their rate is also used for the Fe dielectronic recombination. In addition, we use the photoionization and radiative recombination rates estimated by von Steiger & Geiss (1989) based on cross sections by Vernazza et al. (1981). With these rates, for low-FIP elements photoionization is the

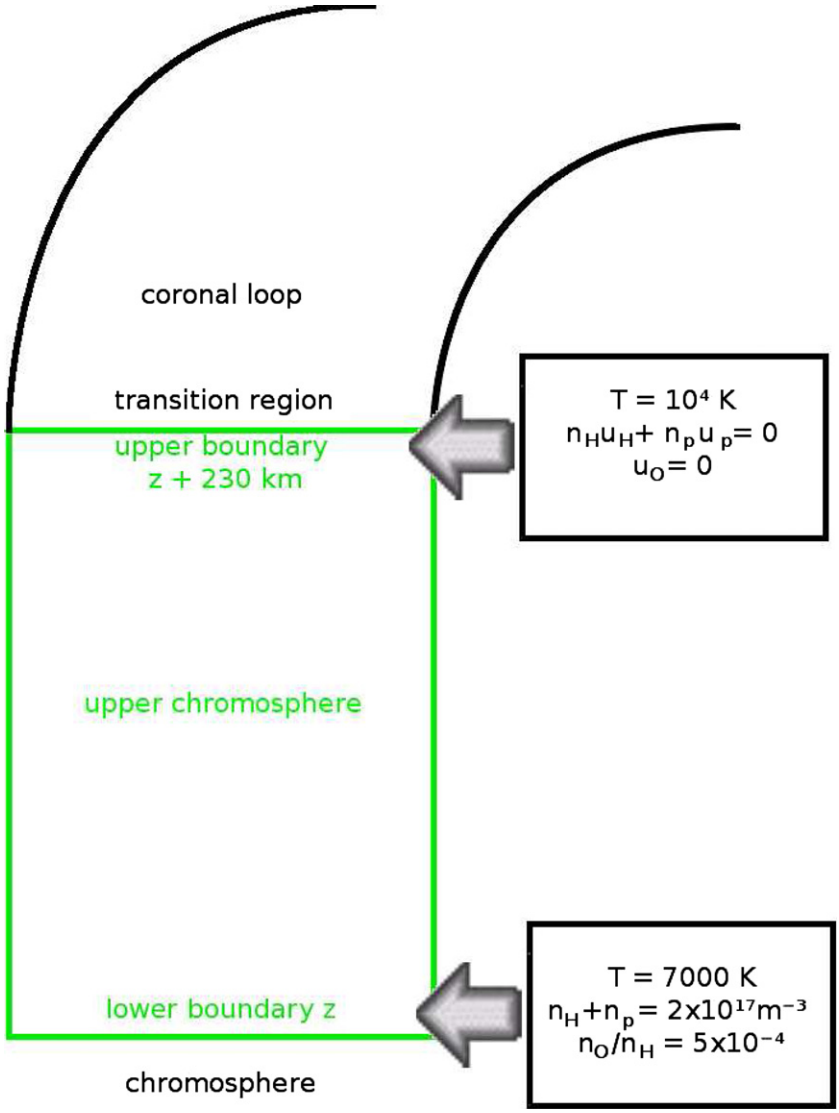

Figure 1. Sketch of the modeled region (colored green), with assumed boundary conditions at the upper and lower boundaries.
(A color version of this figure is available in the online journal.)

dominant ionization process and these elements will basically be fully ionized throughout the upper chromosphere.

For oxygen, resonant charge transfer with hydrogen is a dominant process, determining both the charge state and frictional coupling to hydrogen. Denoting O I by subscript 1 and O II by subscript 2, the rates are

$$P_{12} = n_p C_I \tag{2}$$

$$P_{21} = n_H C_R \tag{3}$$

where the rate coefficients are (Arnaud & Rothenflug 1985)

$$C_I = 9.1 \times 10^{-16} \exp\left(-\frac{19.6 \times 10^{-3}\ \mathrm{eV}}{kT}\right) \times \left[1 - 0.93 \exp\left(-\frac{T}{10^3\ \mathrm{K}}\right)\right]\ \mathrm{m^3\ s^{-1}} \tag{4}$$

$$C_R = \left[1 - 0.66 \exp\left(-\frac{9.3T}{10^4\ \mathrm{K}}\right)\right] \times 10^{-15}\ \mathrm{m^3\ s^{-1}}. \tag{5}$$

At the temperatures of the upper chromosphere $C_I \simeq 9.1 \times 10^{-16}\ \mathrm{m^3\ s^{-1}}$ and $C_R \simeq 10^{-15}\ \mathrm{m^3\ s^{-1}}$. In ionization equilibrium, the oxygen ionization degree is therefore almost equal to the hydrogen ionization degree,

$$\frac{n_2}{n_1} \approx \frac{P_{12}}{P_{21}} \approx 0.91 \frac{n_p}{n_H}. \tag{6}$$

The momentum equation reads

$$\frac{\partial(n_i u_i)}{\partial t} + \frac{\partial(n_i u_i^2)}{\partial z} = -\frac{1}{m_i}\frac{\partial(n_i kT)}{\partial z} + \frac{n_i q_i}{m_i} E - g n_i + \sum_{j \neq i} n_i \nu_{ij}(u_j - u_i) + n_j u_j P_{ji} - n_i u_i P_{ij}, \tag{7}$$

where m_i is the particle mass, k is Boltzmann's constant, $T(z)$ is the temperature, and q_i is the particle charge. The electric field E can easily be derived from the momentum equation of the electrons, $E = -(1/en_p)(\partial(n_p kT)/\partial z)$, where e is the elementary charge and $n_p \approx n_e$. A constant value is used for the gravitational acceleration g since the thickness of the chromosphere is much smaller than the Sun's radius $R_\odot$.

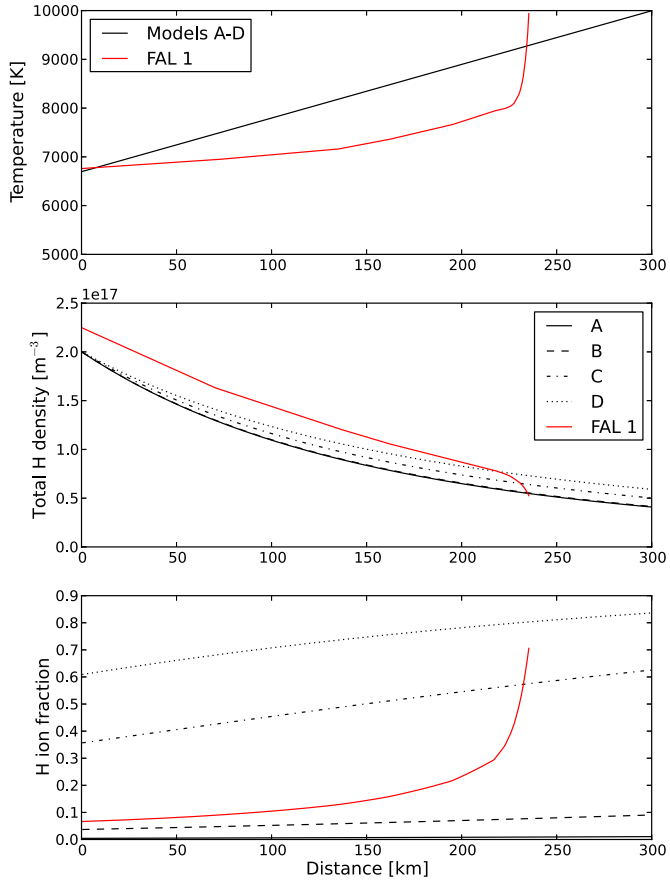

Figure 2. Background temperature, hydrogen density ($n_H + n_p$) and H ion fraction ($n_p/(n_H + n_p)$). "FAL 1" is given by Fontenla et al. (1990, Table 2), which is identical to model C of Vernazza et al. (1981, Table 12) below $T = 7940$ K.

(A color version of this figure is available in the online journal.)

The collision frequencies ν_{ij} represent neutral–neutral, neutral–ion, and Coulomb collisions. Their values are taken from Schunk (1977), with the atomic polarizability (for neutral–ion collisions) and hard sphere cross section (for neutral–neutral collisions) given by Marsch et al. (1995).

For the minor element, the flow speed is set to zero at the upper boundary. Hence, during the gravitational settling, no minor particles will enter the slab from above and the density near the upper boundary must decrease with time. As discussed above, this boundary condition is appropriate when the upper boundary is at the bottom of the transition region. At the lower boundary, the flux of minor species is set equal to the flux at the next grid point above the boundary. This "open" boundary condition allows settling minor particles to leave the slab. However, due to the high H density near the lower boundary, the settling speed is very small here, and the minor element density at the lower boundary will in most cases essentially be frozen at its initial value during the integration time of the model.

At the start of the time integration, the minor element abundance is set to 5×10^{-4} (relative to the total hydrogen density) everywhere. This value is close to the observed oxygen abundance. By setting all elemental abundances initially to the oxygen abundance, we simplify the comparison between elements as, e.g., the abundance of an element relative to oxygen will be a direct measure of the fractionation of that element. Since the minor elements are treated as "test" particles not affecting the hydrogen background, choosing a different initial abundance simply means that the results shown here must be scaled accordingly. The ionization degree is set to 10^{-6} initially. Ionization processes will subsequently quickly change the initial ionization degree.

Table 1
Hydrogen Photoionization Rate and Resulting Ionization Degree between Lower and Upper Boundary for the Four Background Models

Model	R_{Hp} (s^{-1})	Ionization Degree
A	1.9×10^{-6}	0.4%–1.2%
B	1.5×10^{-4}	3.6%–9%
C	2.2×10^{-2}	31%–57%
D	4.1×10^{-1}	61%–84%

For the cases in which we solve the continuity and momentum equations for the hydrogen background (see Section 4), the momentum equation for neutral hydrogen and protons can be cast in the form

$$\frac{\partial(nu)_{H(p)}}{\partial t} + \frac{\partial(nu^2)_{H(p)}}{\partial z} = -\frac{a}{m_p}\frac{\partial(n_{H(p)}kT)}{\partial z} - g n_{H(p)} + n_{p(H)} u_{p(H)} P_{pH(Hp)} - n_{H(p)} u_{H(p)} P_{Hp(pH)} + k_{mt} n_{H(p)} n_{p(H)} (u_{p(H)} - u_{H(p)}), \quad (8)$$

where $a = 1$ for H and $a = 2$ for p (accounting for the electric field contribution). For the friction terms due to elastic collisions we adopt the rate coefficient

$$k_{mt}(T) = 1.9 \times 10^{-14} \sqrt{\frac{T}{10^4\ \mathrm{K}}}\ \mathrm{m^3\ s^{-1}}, \quad (9)$$

which is in good agreement with the momentum transfer rate coefficient provided by Schultz et al. (2008) at chromospheric temperatures. For P_{Hp} and P_{pH} we use the direct ionization and radiative recombination rates provided by Arnaud & Rothenflug (1985), and in addition we have a constant (with altitude) photoionization rate, specified in Table 1.

In the hydrogen calculation, the density is initially set to $n_H + n_p = 2 \times 10^{17}$ m^{-3} at the lower boundary and decreases with the scale height of neutral hydrogen, corresponding to hydrostatic equilibrium for neutral H. The ionization degree is initially set to 10^{-4}. The hydrogen model is typically integrated, using a semi-implicit scheme, for 10^6 s, allowing for a steady state solution to be reached. The density profile will change slightly compared with the initial profile caused by ionization (protons have a larger scale height than neutral H due to the electric field).

At the upper boundary, the net hydrogen flux is set to zero, ensuring that in steady state there will be no net hydrogen flow through the slab. At the lower boundary, pressure perturbations are allowed to pass through, using the scheme of Korevaar & van Leer (1988), so that the prescribed density of 2×10^{17} m^{-3} is maintained in steady state.

3. COULOMB FRICTION IN A "TYPICAL" SOLAR ATMOSPHERE

To demonstrate the effect of Coulomb collisions on different elements, we first choose the FAL 1 atmospheric model for the hydrogen background given by Vernazza et al. (1981) and Fontenla et al. (1990). This is a semiempirical model which

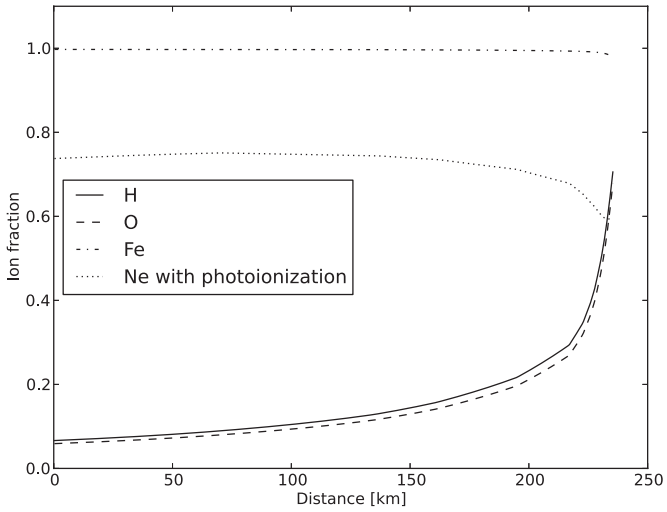

Figure 3. Ion fraction for hydrogen, oxygen, iron, and neon in the FAL 1 background.

includes ambipolar diffusion, and where the temperature profile is obtained from measured EUV intensities. It describes the average quiet sun. This background is shown in Figure 2 (models A–D will be discussed in Section 4). In this case, we put the upper boundary of our model, used for the minor species, at approximately $z = 230$ km where $T \approx 10^4$ K, since we consider this to be the start of the transition region where our model does not apply.

With this given background, we solve the minor element continuity and momentum equations given in Section 2. Figure 3 shows the modeled ion fraction for oxygen, iron, and neon in the FAL 1 background. With the chosen ionization and recombination rates, ionization equilibrium is reached almost instantly, and essentially remains constant during the gravitational settling. We note that the oxygen ionization closely follows that of hydrogen, due to the resonant charge exchange between oxygen and hydrogen, and is to a very good approximation given by Equation (6). At the lower boundary, the ionization degree of the chromosphere is about 5%, and it rises to about 70% at the top of this model in the upper chromosphere. Because of the photoionization rate used, iron is fully ionized throughout the slab. Note also that with the chosen photoionization rate (from von Steiger & Geiss 1989), neon is almost 80% ionized throughout the upper chromosphere and has a much higher ionization degree than hydrogen and oxygen, despite the fact that neon has a much higher FIP than H and O. For this reason we have also run the neon model without photoionization (only direct ionization), and the neon ion fraction is then less than 10^{-7} throughout the slab. The ion fractions, with Ne photoionization, are in approximate agreement with those obtained by Laming (2004).

In Figure 4, the upper panel, we have plotted the absolute abundance of Fe and O at different time steps as a function of height, and one can clearly see the effect of gravitational settling. In the uppermost 100 km of the chromosphere, the oxygen abundance has decreased by a factor 2–10 (depending on altitude) after 3 hr, while the iron abundance has changed little below 200 km. (The initial, short-lived increase in the O absolute abundance at the upper boundary is an artifact of the boundary condition, preventing upstreaming O I from leaving the slab.) In the lower panel, we show the ratio of the Fe density to the O density at the same time steps. Because of the large reduction in the O abundance, shown in the upper panel, the

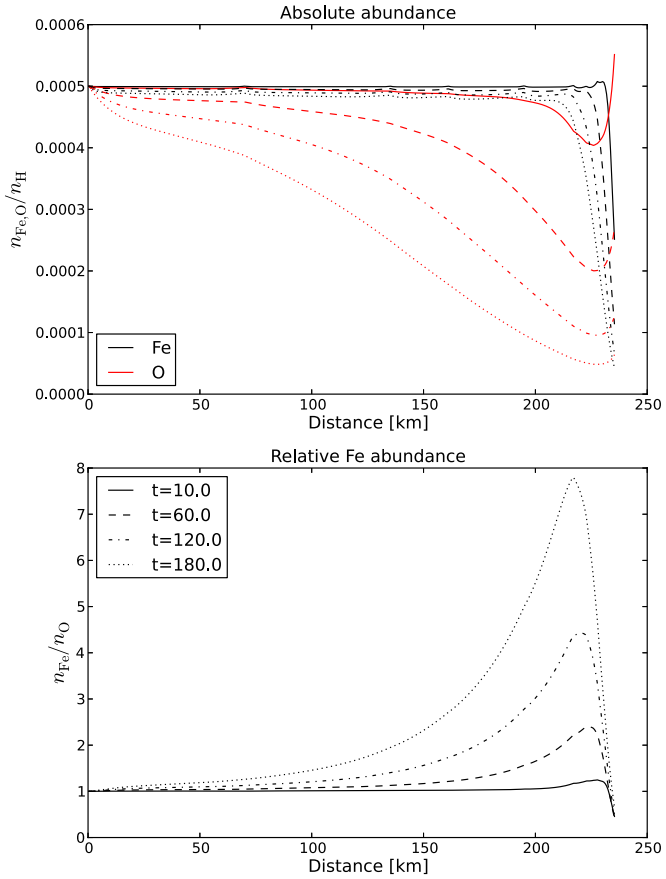

Figure 4. The absolute iron and oxygen abundances, $n_{\mathrm{Fe,O}}/(n_{\mathrm{H}} + n_p)$ (top panel), and the iron abundance relative to O, $n_{\mathrm{Fe}}/n_{\mathrm{O}}$ (bottom panel), for the FAL 1 background model of Figure 2. The time in the legend is given in minutes. (A color version of this figure is available in the online journal.)

iron abundance relative to oxygen increases strongly with time as the gravitational settling progresses. The reason for this is that iron is almost fully ionized throughout the modeled altitude region, while oxygen only becomes almost fully ionized near the upper boundary. The Coulomb friction between Fe ions and protons causes iron to settle much more slowly than O ions, despite the fact that iron has an atomic mass more than three times that of oxygen. In most of the slab, hydrogen is more than 80% neutral. However, because the Coulomb cross section at these temperatures is of the order of 10^3 times the ion–neutral and neutral–neutral cross section, the interaction between iron and hydrogen is still dominated by Coulomb collisions. Had it not been for Coulomb collisions, the heavier Fe would have been depleted relative to O.

The abundance enhancement of Fe relative to O keeps increasing with time and can be very significant. For example, if no mixing takes place that removes material from the box and into the corona, then after 1 hr the abundance ratio of Fe to O is more than a factor of two at the highest heights. After 3 hr of undisturbed settling, the iron relative abundance reached a maximum of more than 7. The effect at the lower heights is quite small. If we run the model much longer, then the relative abundance increases monotonically with time, and after 11 hr it reaches values of more than 300. After such long settling times, the relative iron abundance near the bottom of the model has also increased substantially (with, e.g., a relative abundance of 10 at $z = 50$ km). In this model, the iron settling velocity is nearly constant with altitude, except near the upper boundary

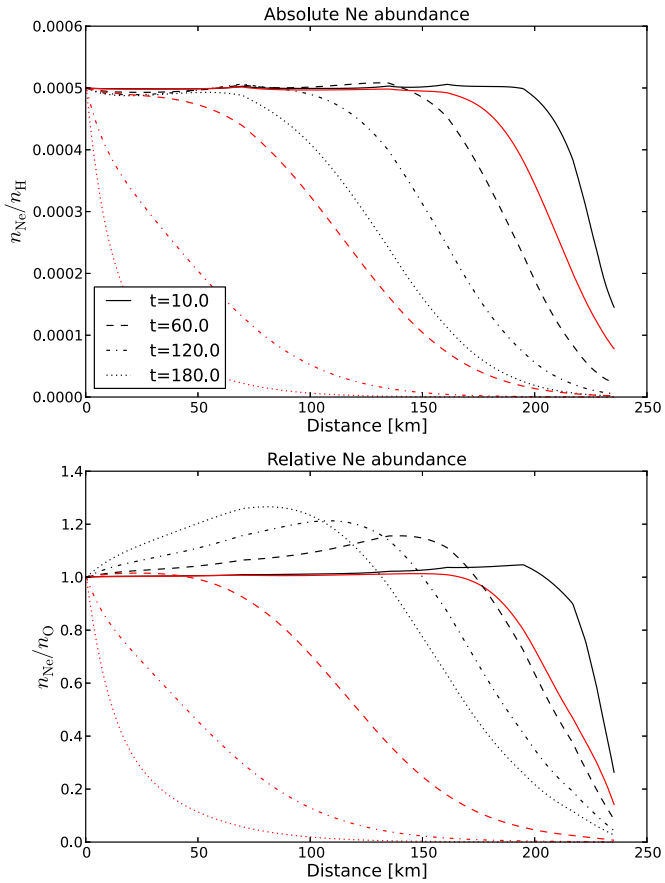

Figure 5. The absolute neon abundance $n_{Ne}/n_H + n_p$ (top panel) and the abundance relative to O, n_{Ne}/n_O (bottom panel), for the FAL 1 background model of Figure 2. The time in the legend is given in minutes. Black curves were computed with Ne photoionization while red curves were computed without (direct ionization only).

(A color version of this figure is available in the online journal.)

(where it is reduced); the higher H density at lower altitudes is accompanied by a reduced H ionization degree, and hence a smaller mean collision frequency between H and Fe^+ ions. This implies that the downward flux of Fe actually monotonically increases with decreasing altitude (because the Fe density is higher at lower altitudes). From the continuity equation (1) the Fe density will then decrease in time at all altitudes, and there will never be a "pile up" of iron at lower altitudes. However, because the Fe density is higher at lower altitudes, a longer time is required there to obtain, e.g., a 50% decrease in the Fe density. The temporal increase in the Fe relative abundance seen in Figure 4 is thus caused solely by the decrease in O density everywhere.

As a comparison, we have carried out the corresponding calculations for the high-FIP element Ne. The results are shown in Figure 5 both with and without Ne photoionization. Even with photoionization the lower ionization degree of Ne relative to Fe leads to a gravitational settling which is much larger and increases more rapidly with time than in the case of Fe. With photoionization the abundance of Ne relative to O (lower panel) is increased slightly at the lower heights but is significantly depleted relative to O at the upper heights. Without photoionization neutral neon sinks rapidly and is quickly and strongly depleted both relative to hydrogen and to oxygen.

Figure 5 illustrates that even if the high-FIP element neon were substantially more ionized than oxygen (see Figure 3), neon would still become depleted relative to oxygen in the upper chromosphere, and the enhancement relative to oxygen in the lower part is small. Also, relative to iron, neon would become strongly depleted in the upper chromosphere. The main cause of the depletion is the substantial fraction of neutral neon present, even with photoionization. Second, neon has a smaller collisional cross section than both oxygen and iron (except for Coulomb collisions). We have rerun the neon model with photoionization, but using the oxygen collision cross sections, and this causes the maximum relative neon abundance (after 3 hr) to increase from 1.25 (lower panel of Figure 5) to 1.7 (not shown in the figure), and the depletion relative to O in the uppermost region to become much smaller. This shows that some fractionation can be caused by atomic size effects, although the ionization degree has a significantly larger impact on the fractionation.

Figures 4 and 5 indicate that the upper chromosphere can become substantially enriched in low-FIP elements relative to high-FIP elements such as neon and oxygen. We chose Fe as the low-FIP element because it is heavy, with an atomic mass approximately a factor of three greater than that of oxygen and neon, and hence the most "difficult" element to enrich by gravitational settling. The enrichment would be even larger for lighter low-FIP elements, such as magnesium and silicon.

In order to cause an enhancement of Fe relative to O in the corona, the chromospheric material needs to be transported into the corona. As mentioned, we assume that some process, e.g., reconnection or heating by sound waves, sporadically heats the chromospheric material converting it into coronal plasma. The elemental composition of this newly created coronal matter will depend on how long the chromospheric gravitational settling has been going on, but it will also depend on how much of the chromosphere is converted into coronal matter. If only the upper 20–30 km of the chromosphere, say, are converted into coronal plasma, Figure 4 shows that a high coronal Fe abundance (relative to O) may result. On the other hand, a large amount of heating that expels the upper 200 km of the chromosphere will create coronal plasma with little enrichment since little FIP-enhancement is obtained 200 km below the top of the chromosphere (where densities are much higher, too). In order to estimate the effect of chromospheric gravitational settling on coronal abundances, we can compute the *average* chromospheric absolute and relative abundance of minor element i as

$$a_i(z,t) \equiv \frac{\int_z^{z_t} dz'\, n_i(z',t)}{\int_z^{z_t} dz'\, (n_H(z',t) + n_p(z',t))} \tag{10}$$

$$r_i(z,t) \equiv \frac{\int_z^{z_t} dz'\, n_i(z',t)}{\int_z^{z_t} dz'\, n_O(z',t)}, \tag{11}$$

where z_t is the altitude of the top of our slab (and the top of the chromosphere), n_i is the total minor element density (sum of the neutral and singly ionized density), and $n_H + n_p$ and n_O the total hydrogen and oxygen density, respectively. Figure 6 shows $a_{Fe}(z,t)$ and $r_{Fe}(z,t)$ for the Fe and O solutions shown in Figure 4 and at the same time steps. It can be seen that, e.g., after 2 hr of gravitational settling, if the chromosphere above $z = 200$ km altitude is ejected into the corona, then this material will have a relative iron abundance $r_{Fe}(z = 200\ \text{km}) \approx 3$, while $r_{Fe}(z = 100\ \text{km}) \approx 1.7$. In other words, even if the uppermost 100 km or so of the chromosphere is "evaporated," the resulting coronal material will still have a substantial enrichment of iron relative to oxygen. The upper panel of Figure 6 shows that even

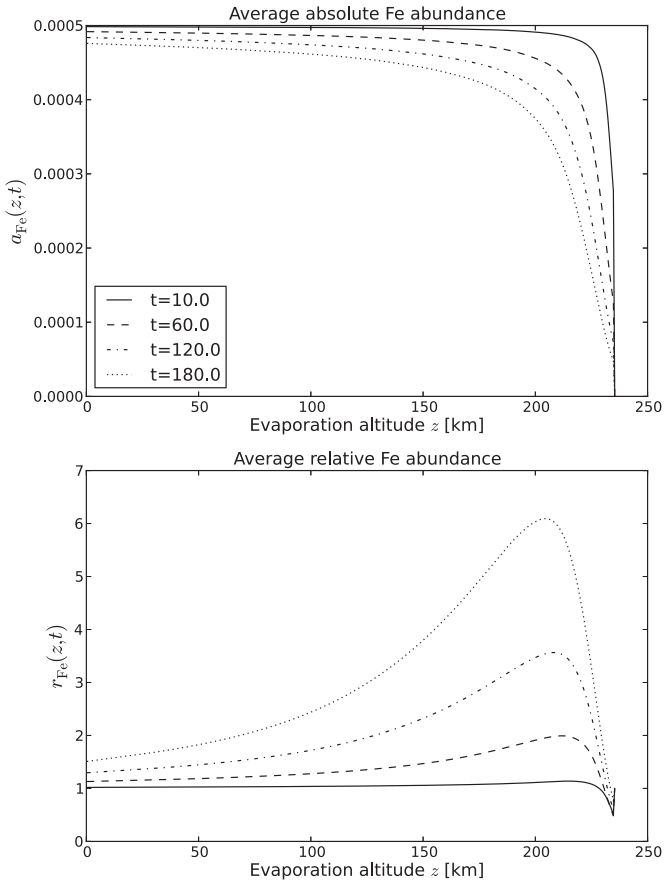

Figure 6. The mean iron composition of the plasma above the given altitude, $a_{\mathrm{Fe}}(z,t)$ and $r_{\mathrm{Fe}}(z,t)$ as defined by Equations (10) and (11), for the solution in Figure 4. These express the average composition of the material above the given altitude and thus the coronal abundance if the material down to this altitude (denoted "evaporation altitude") were expelled into the corona and mixed.

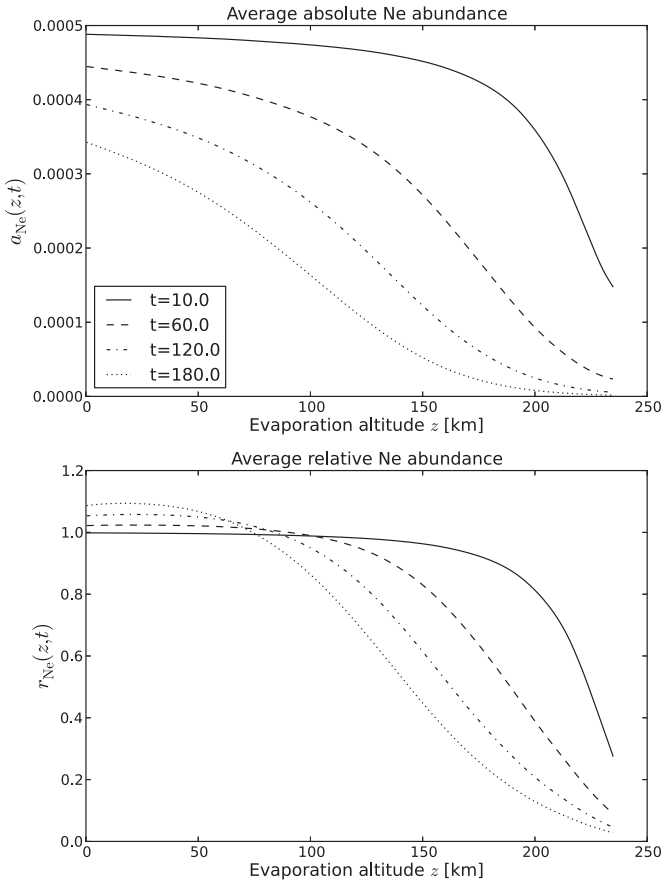

Figure 7. The average neon absolute and relative abundance $a_{\mathrm{Ne}}(z,t)$ and $r_{\mathrm{Ne}}(z,t)$ for the solution in Figure 5 with photoionization and at the same times.

after 2 hr of settling, the average absolute abundance of iron in the uppermost 100 km of the chromosphere has only been depleted by about 10% from its initial, "photospheric," value, while the chromosphere above 200 km altitude has lost about 20% of its initial Fe atoms.

At the same time, $t = 2$ hr, the abundance of the high-FIP element Ne, shown in Figure 7, will have decreased to 0.95 relative to O (lower panel) if the upper 100 km of the chromospheric material is expelled in an event, and to 0.2 if the event ejects the upper 200 km. For the Ne model run without photoionization (see Figure 5), r_{Ne} and a_{Ne} are even much lower than the average abundances shown in Figure 7. Even with the very high photoionization rate of von Steiger & Geiss (1989; causing Ne to become more ionized than H and O), it seems difficult to avoid a depletion of Ne in the upper part of the modeled region.

4. DEPENDENCE OF THE ABUNDANCES ON THE HYDROGEN BACKGROUND

The above examples show that a significant enrichment/depletion of low/high-FIP elements can be achieved relative to O due to the combination of gravitational settling and Coulomb collisions. The resulting abundances depend on the properties of the background chromosphere, primarily on the ionization degree of hydrogen, as well as on the properties of the heavy ions (mass and ionization degree). With very little background (hydrogen) ionization, the ionization degree of the minor element should have little impact on the gravitational settling (and hence the abundance) since Coulomb collisions are not important (and neutral–neutral and ion–neutral cross sections are similar). At the other extreme, with very high hydrogen ionization, oxygen will also be highly ionized (from resonant charge exchange) and consequently oxygen will settle very slowly, making it difficult for heavier elements with a lower FIP than oxygen to become enriched relative to oxygen. So high and low background ionization should lead to little enrichment of heavier elements, while we showed in Section 3 that for a background ionization from the semiempirical FAL 1 model, between these two extremes, substantial enrichment could be achieved.

We will, therefore, now explore how the background ionization affects the settling of the heavy ions using four different modeled hydrogen chromospheres that mainly differ in their ionization degree. The ionization degree of hydrogen is increased from model A to D by increasing the photoionization rate of hydrogen (see Table 1). To focus on the effect of the H ion fraction, we use the same linear temperature profile in all four models, shown in the upper panel of Figure 2. The resulting H density and ionization degree, obtained by integrating the H and p continuity and momentum equations (1) and (8) until steady state is reached, are shown in Figure 2 together with the FAL 1 model. We note that the total H density varies little between the models, the small change being caused by the electric field which matters at high ionization degree. The ionization degree varies from 0.4% at the bottom of model A to 84% at the top of model D, as summarized in Table 1. Models C and D have such

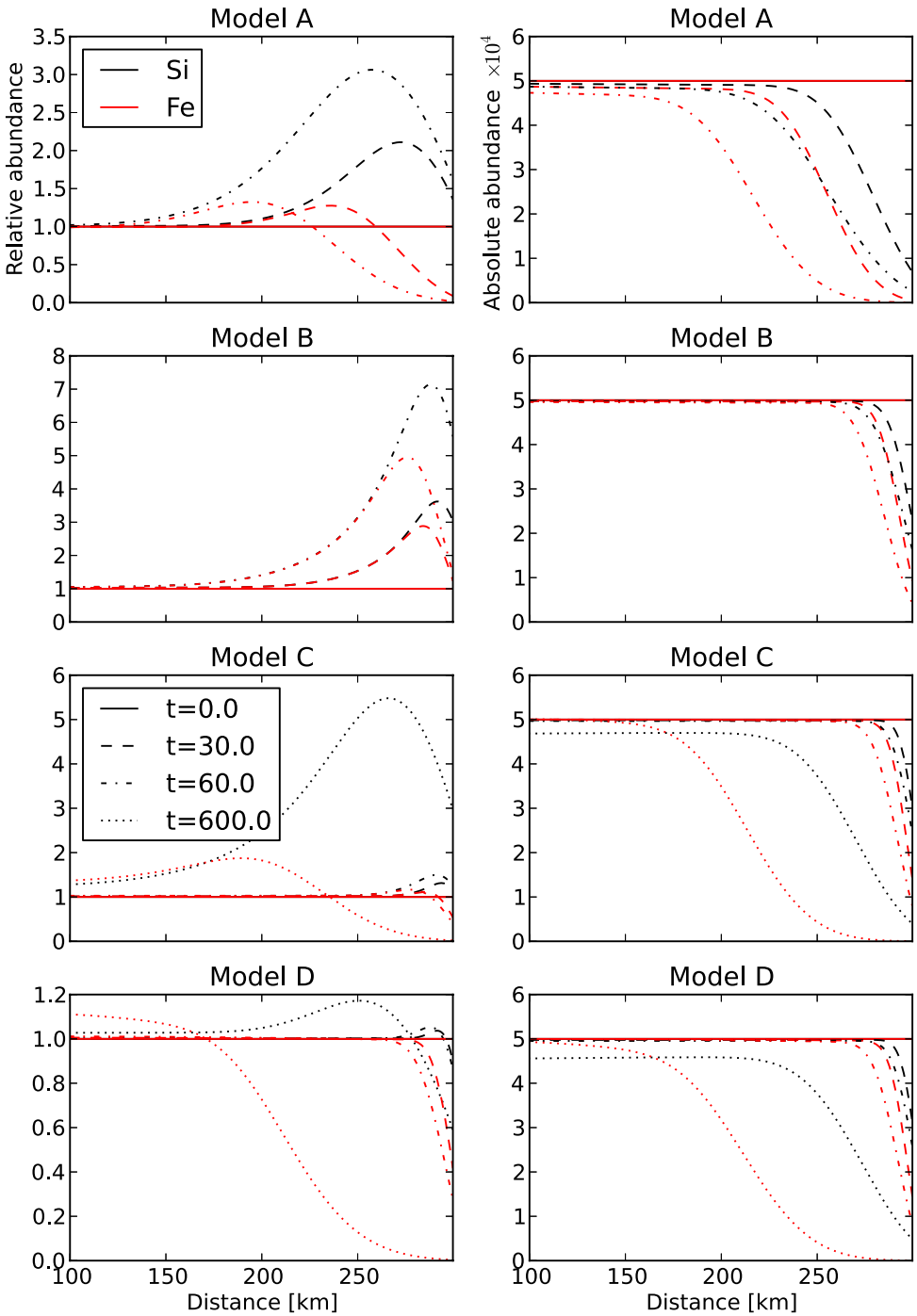

Figure 8. Abundances relative to O (left column) and absolute abundances multiplied by 10^4 (right column) for Si (black) and Fe (red) in models A–D, with times given in minutes.

(A color version of this figure is available in the online journal.)

high ionization degrees that they are hardly compatible with a chromosphere; had we included the energy equation, it would have been difficult to balance heating with radiative cooling at such ionization degrees and a transition region and corona would most likely have formed. These are therefore not meant as realistic chromospheric models, but rather meant to explore the effect of the background ionization on element fractionation.

We will focus on the behavior of the low FIP-elements Fe and Si relative to H and O. The two elements have very similar ionization potentials (7.9 eV and 8.1 eV, respectively) and both are essentially fully ionized in the models considered here. However, Fe is about twice as heavy as Si and since the Coulomb collision frequency is inversely proportional to the mass of the heavy ion, the collision frequency of Si^+ with protons is twice the Fe^+ collision frequency.

The results of the model calculations are shown in Figure 8. Below 100 km (not shown in the figure), the coupling of the ions to hydrogen is so strong due to the high density that gravitational settling is prevented almost entirely.

In model A, with an H ionization degree varying from 0.4% at the lower boundary to 1.2% at the upper boundary, the effect of gravitational settling can be seen in both Fe and Si above a height

of 200–250 km. However, even after one hour, appreciable amounts of Si and Fe are still present in the slab, although Fe is then severely depleted above 250 km. The ionization degree of O follows very closely that of H (see Equation (6)), and with such a low ionization degree Coulomb collisions are much less efficient in preventing the settling of O. For this reason we can see a strong increase of the Si density relative to O, about a factor of three at a height of 250 km after one hour (while the absolute abundance has decreased by 50%). Also, Fe increases relative to O but that increase is rather modest due to the larger mass and consequently smaller Coulomb collision frequency compared with Si.

In model B, the ionization degree of hydrogen is increased by about a factor of 10 over the whole height range (see Table 1). This is of course also true for O which follows H. However, the increased ionization degree of O is not sufficient to couple O efficiently to the background and O continues to settle almost as fast as in model A. The low-FIP elements Si and Fe remain basically fully ionized, although there is a small reduction in the ionization degree (by roughly 1%) compared with model A, caused by the increased recombination rate which is proportional to n_p. The increase in the Coulomb collision frequency, which is proportional to n_p, results in a significant slow down of the gravitational settling of Fe and Si relative to model A. Up to a height of 250 km, Fe and Si show hardly any signs of gravitational settling even after one hour (as seen in the absolute abundance in Figure 8). The abundances of Fe and Si relative to O therefore markedly increase and reach maximum values of about 5 and 7, respectively, above 250 km. This behavior of the three elements can best be understood by comparing the downward velocities. In model B, the downward velocities of Si and Fe are less than the O flow velocity (averaged over charge states) over the entire slab, and an increase of the Si and Fe abundance over O is established quickly and will keep increasing with time. In model A, the Si over O velocity is still less than 1, while the Fe over O velocity is only marginally smaller than 1 in a very narrow region of the slab.

Further increasing the ionization degree of H to values too large to be consistent with a chromosphere, models C and D (included for demonstration purposes) slow the gravitational settling of all three elements and it takes much longer before relative abundance differences start to develop. The panels for models C and D in Figure 8 therefore also include the time $t = 10$ hr. After 10 hr, appreciable amounts of Si and Fe are still present in the slab. Even though the ionization degree of O is increased from model B to C, Coulomb collisions are still not able to prevent O from falling faster than Si and Fe in part of the chromosphere, so that the maximum abundance ratio of Si to O still reaches a value of about 5. The increase of Fe over O is rather modest, about 1.5 after 10 hr. The peaks where these maxima occur have now moved to lower heights. Running the calculations for an even longer time will increase the maximum values of the abundances and move these maxima even closer to the lower boundary. However, after 20 hr, for example, very little of the heavy elements is left in the slab. Finally, in model D, the ionization degree of O is so high that Coulomb collisions are strong enough to also slow down the settling of O, which now falls slower than both Si and Fe in almost the whole slab and neither Si nor Fe are enhanced over O.

To see what the abundances that one could expect in the corona are, we again assume that the upper part of the atmosphere is ejected, caused, e.g., by sudden heating or reconnection. Figure 9 shows the average abundances (defined by Equations (10) and (11)) above the given evaporation altitude, resulting from the abundances of Figure 8, providing a measure of the elemental composition of this gas if it is expelled into the corona. The figure shows that if the settling process has been taking place for one hour, the absolute average abundance above an evaporation altitude of 200 km is still sizable, except for iron in model A. In model A, the Si abundance relative to O clearly shows an increase even if only a small fraction of the atmosphere is removed. Iron, on the other hand, shows no enrichment in model A no matter how much of the atmosphere is removed. In model B, enrichment of Si relative to O by factors of four to seven could result, depending on how much material is removed and after what time interval the ejection takes place. The enrichment of Fe relative to O could be as much as a factor of three in model B if the material is ejected after one hour. In model C, a small enhancement of Fe relative to O can be achieved in the corona if the ejections take place on much longer time scales and a much larger part of the atmosphere is ejected compared to model B. In model D, no enrichment of Fe relative to O can be achieved and the enrichment of Si relative to O is negligible.

5. DISCUSSION AND SUMMARY

The calculations carried out for the FAL 1 model and models A–D show not only that Coulomb collisions can greatly affect the abundances of high- and low-FIP elements relative to each other, but also that this effect is sensitive to the hydrogen ionization degree and that there is an "optimum" ionization degree of H (and O) where the effect is most pronounced. This optimum is close to the FAL 1 model (Fontenla et al. 1990) and model B, with ionization degrees varying from 5%–10% up to 20%–30%.

For the mechanism to produce significant abundance enhancement of low-FIP elements relative to O, the low-FIP elements must have an ionization degree higher than that of H and O, and for heavy elements, such as iron, it must be much higher. In the models presented here, photoionization, using the rates given by von Steiger & Geiss (1989), ensured that the low-FIP elements were basically fully ionized in the chromosphere. We have rerun model B with photoionization switched off for Fe and Si. In that case, the ionization degree of Si is still about 90% and the Si/O abundance enhancement reaches a value of about four after one hour, compared with a factor seven with photoionization (see Figure 8). Without photoionization, the Fe ion fraction varies from about 40% at the lower boundary to about 85% at the upper boundary, and the maximum ratio of Fe/O decreases in this case to about 1.4 after 1 hr (while it reached a maximum of almost 5 with photoionization as seen in Figure 8). In other words, if this process is to produce iron relative enhancements in approximate agreement with observations, then a high ionization degree for iron is required, of the order of 90% or more, and this cannot be obtained without a high photoionization rate.

Apart from its influence on abundances (element fractionation), the main effect of increasing the H ionization degree is that the time scale necessary for significant fractionation increases. Even going from model A to B, both having quite low ionization degrees, the amount of settling after one hour, say, is strongly reduced, as seen in the absolute abundances of Figure 8. If this process—gravitational settling followed by ejection into the corona—is to produce coronal relative abundances comparable to observations, then the required time between ejection

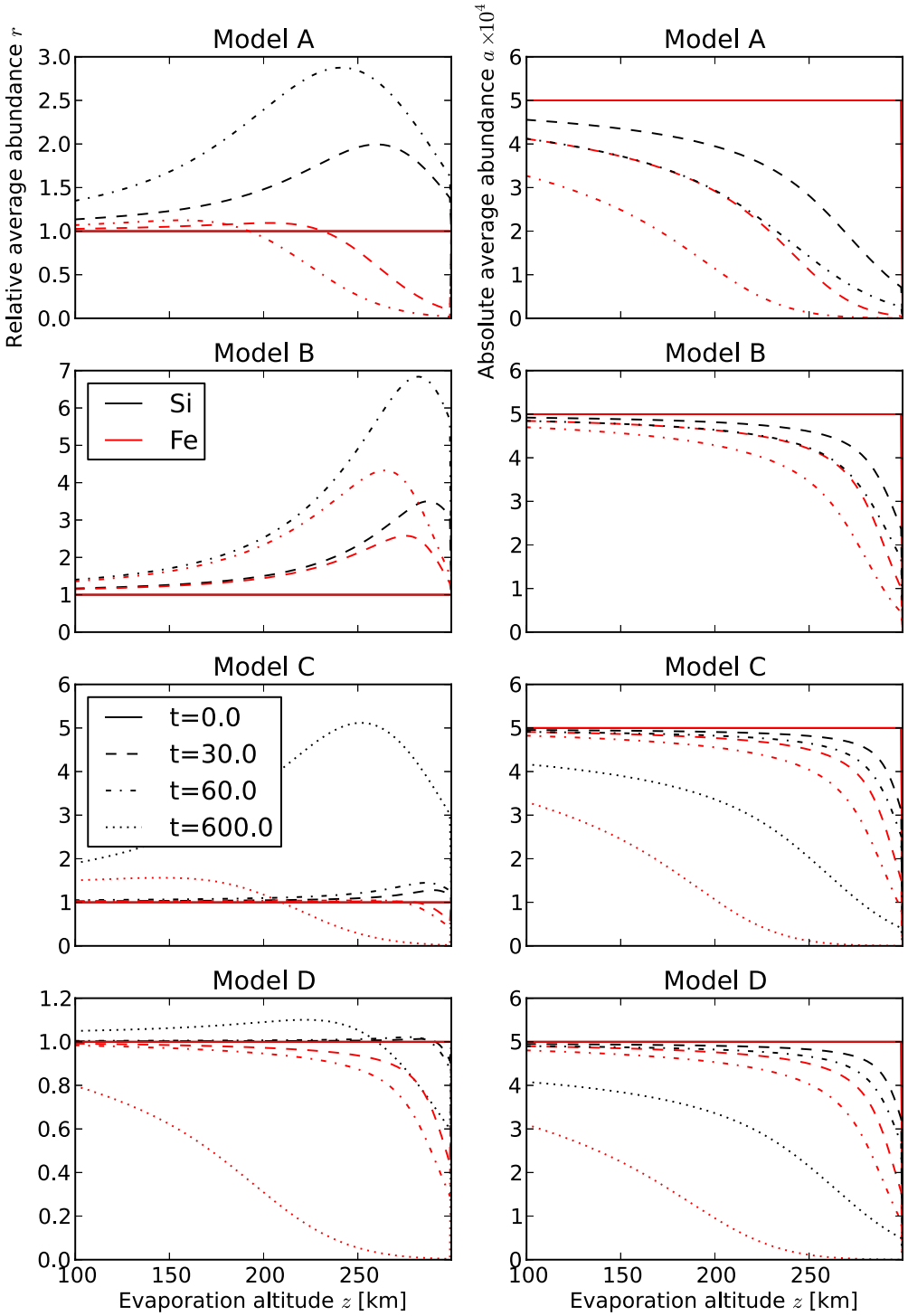

Figure 9. Relative average abundances ($r_{\rm Ne}$, $r_{\rm Fe}$) (left column) and absolute average abundances ($a_{\rm Ne}$, $a_{\rm Fe}$) multiplied by 10^4 (right column), for Si (black) and Fe (red) in models A–D, similar to Figures 6 and 7 for the FAL 1 model. The times are given in minutes.

(A color version of this figure is available in the online journal.)

events must be much longer for a highly ionized chromosphere than for a low ionization degree. With the ionization degree of the FAL 1 model, and provided the uppermost ∼50 km is ejected, one to two hours between events would be required to produce coronal relative Fe abundances in approximate agreement with observations (see Figure 6). On the other hand, observations show that the coronal FIP bias can build up over days to values much larger than the typical value of four (Widing & Feldman 2001), which would require much longer ejection intervals.

A problem with the photoionization rates of von Steiger & Geiss (1989) is that neon becomes highly ionized in the chromosphere despite a FIP of about 22 eV; in the FAL 1 background, neon is more than 70% ionized (Figure 3). Hence, neon has an ionization degree much higher than that of H and O, despite the fact that the FIP for neon is much higher. One may

therefore argue whether or not such high neon photoionization rates are realistic in the chromosphere. The origin of these "hard" photons is presumably backradiation from the corona. The rates computed by von Steiger & Geiss were obtained from the observed solar UV spectrum at 1 AU, not taking into account absorption in the transition region and upper chromosphere. We therefore used two models for neon, one with photoionization and one completely without (i.e., only including direct ionization). In the latter, the neon ionization degree is extremely small and neon is rapidly and strongly depleted in all models, as shown in Figure 5. However, even with the chosen photoionization rate, which may be unrealistically high, neon would be depleted in the upper chromosphere, although much less so than without photoionization. This depletion is partly caused by the ∼30% neutral Ne still present, and partly by the neon atom being "small": both the atomic radius, entering the neutral–neutral collision frequency, and the atomic polarizability, entering the neutral–ion collision frequency, are smaller for neon than for oxygen, silicon, and iron. This compensates for neon being much lighter than silicon and iron, and results in a higher settling speed for neon. To conclude, we find that neon tends to become depleted (relative to O and low-FIP elements), even with a very high neon ionization degree (much higher than that of O). A neon relative abundance enhancement would only occur in the hypothetical case where neon is almost fully ionized, which requires an even higher photoionization rate than used here. A faster gravitational settling of Ne in the upper chromosphere seems almost unavoidable. This would also lead to a Ne/O ratio in the corona smaller than the photospheric value assumed at the lower boundary of the model. Additional gravitational settling in the corona will enhance the discrepancy between coronal and photospheric values. The calculations carried out in the present paper seem to support the ideas of, e.g., Bahcall et al. (2005) and Drake & Testa (2005), namely that the coronal Ne/O ratio might be higher in the photosphere than in the corona.

In the model calculations, we have assumed a background chromosphere in hydrostatic equilibrium and with no net hydrogen flow. This assumption can be appropriate for the chromosphere underlying, e.g., the streamer region with closed coronal loops. However, it may not be appropriate for the part of the chromosphere underlying the source region(s) of the solar wind. In particular, it will be inappropriate for the part of the chromosphere underlying the fast solar wind originating in coronal holes. In this latter region, the hydrogen outflow will counteract gravitational settling of minor elements, and if the chromospheric outflow speed is sufficiently high, as it will be for a wind emanating from coronal funnels, then the settling will be inhibited entirely (Pucci et al. 2010). In that case, the model used here would have produced no enhancements or depletions, neither relative to hydrogen nor to oxygen, and the solar wind material would have close to photospheric abundances. Observations show that the FIP-effect in the fast solar wind is either small (von Steiger et al. 2000) or absent, with the exception of helium and, probably, neon, which are both depleted (Gloeckler & Geiss 2007).

Although relative abundance enhancements in the upper chromosphere can readily result from the gravitational settling process, this does not automatically imply similar abundances in the corona. An independent process not included in our model must heat and ionize the upper chromosphere. Possible mechanisms could be reconnection in the corona followed by a strong increase in downward heat conduction into the chromosphere, or direct heating of the upper chromosphere, e.g., by upward-propagating sound waves. Such processes could also cause a remixing of the chromosphere, counteracting the effect of gravitational settling. Because the temperature is increasing with altitude in the upper chromosphere, this region is convectively stable. Hence, an external process is necessary to do the mixing. The (additional) heating of the upper chromosphere cannot take place too frequently or too rarely: if it happens too frequently—say, with only a few minutes intervals—then the heavy elements will not have time to undergo significant gravitational settling and the resulting coronal abundances would be close to photospheric. If it happens only rarely (intervals of several hours or more), then the resulting coronal plasma will be depleted in all heavy elements, and particularly in the high-FIP elements.

We have found that if, e.g., the uppermost 100 km of the chromosphere is heated and turned into coronal plasma, then this plasma can have iron relative abundance enhancements of the order of three to four if the chromosphere has been allowed to gravitationally settle for three hours or so (Figure 6). Although the heating process is beyond the scope of our model, we may still ask whether it is realistic that the uppermost 100 km of the chromosphere is "suddenly" converted into coronal plasma? The location of the interface between the top of the chromosphere and the transition region is determined by the radiative energy balance in the transition region. Downward heat conduction from the corona is used to heat plasma streaming up from the chromosphere into the corona and to balance radiative loss in the transition region. In a steady state with no net flow (which can be an appropriate assumption in closed field regions), all the heat flux is lost as radiation and it can be shown that the pressure in the transition region, which equals the pressure at the top of the chromosphere, is directly proportional to the downward heat flux density (Landini & Monsignori Fossi 1975),

$$P_t \approx C q_m, \tag{12}$$

where q_m is the downward heat flux density in the low corona (or upper transition region). The constant of proportionality C is determined by the radiative loss function employed. Assuming that the transition region is optically thin and using the loss function of Rosner et al. (1978), the constant has been found to be (Hansteen & Leer 1995)

$$C \simeq 7.5 \times 10^{-5}\ \mathrm{s\ m^{-1}}. \tag{13}$$

Taking our model B as an example, the hydrogen density at the top of the slab is $n_{\mathrm{H}} \approx 4 \times 10^{16}\ \mathrm{m^{-3}}$ and the temperature is 10^4 K (Figure 2), and hence $P_t = 5.5 \times 10^{-3}$ Pa (the H ion fraction is low so the electron pressure can be omitted). From Equations (12) and (13), this implies a downward heat flux $q_m \simeq 73\ \mathrm{W\ m^{-2}}$. This value is roughly equal to the energy flux density needed to drive the observed solar wind, assuming a radially expanding flow geometry. As shown by Hansteen & Leer (1995), most of the energy deposited in a magnetically open corona will be lost in the solar wind (and not as radiation), and the solar wind therefore gives a good measure of the amount of coronal heating taking place in open regions of the Sun. If the coronal heating is not very different in open and closed regions, then one would therefore expect that of the order of $100\ \mathrm{W\ m^{-2}}$ is deposited also in loop regions, and most of this energy is conducted into the transition region. Hence, the density at the top of the chromosphere in all our models is consistent with the amount of heating expected in such a "quiet" corona.

How much extra coronal heating would then be required to move the top of the chromosphere downward by 100 km? In model B, the pressure at 200 km altitude (again see Figure 2) is $P_t \approx 9 \times 10^{-3}$ Pa, which from Equation (12) translates into a downward heat flux density $q_m = 116$ W m^{-2}. During the evaporation phase, the downward heat flux has to be somewhat larger than this (accounting for ionization and heating of the gas), but it indicates that a ∼50% increase in the coronal heating rate is all that is required to expel the uppermost 100 km of the chromosphere. Even if we wanted to expel the whole modeled slab region (the uppermost 300 km of the chromosphere), $q_m \approx 250$ W m^{-2} would be required, less than a factor four increase above the quiet corona heating rate. The actual coronal heating must be expected to be a dynamic process, whether it is caused by waves propagating along field lines into the corona or by reconnection in the corona. During explosive events, such as coronal mass ejections (CMEs) and associated flares, there is evidence that the local heating rate must be orders of magnitude larger than the quiet heating rate, as indicated, e.g., by the very high charge states measured in some CMEs (Lepri et al. 2001). It would therefore be surprising if the heating rate does not often fluctuate in time by 50% or more in localized regions of the corona. Based on this, the location of the top of the chromosphere should move by 100 km or more equally often, and one would expect expulsion of chromospheric material into the corona (as well as the reverse process) to happen regularly without requiring large, explosive events such as flares or CMEs. Indeed, the latter would probably erode so much of the chromosphere that the resulting plasma would have little FIP fractionation, at least from the gravitational settling process considered here.

The relative abundance enhancements always come at the expense of a reduction in the absolute abundance, since gravitational settling can never cause enhancement relative to hydrogen. If relative enhancements of the same magnitude as observed relative abundances require such long settling times that the upper chromosphere becomes almost devoid of heavy elements, then the coronal plasma resulting from expulsion of the upper chromosphere would have absolute abundances much lower than photospheric abundances. However, we find that the reduction in absolute abundance can be quite modest. For instance, from Figure 6 we note that if, after two hours of settling, the uppermost 30 km of the chromosphere is expelled into the corona, the resulting plasma will have an average iron abundance relative to oxygen of about three, while the absolute iron abundance has decreased by less than 20%. In other words, this mechanism is capable of producing significant enhancement of low-FIP elements relative to high-FIP minor elements, while the absolute iron abundance is still close to the photospheric abundance. However, an abundance enhancement relative to oxygen does require that oxygen becomes depleted, as shown in Figure 4. Observations with the Ultraviolet Coronagraph Spectrometer (UVCS) on the *Solar and Heliospheric Observatory* (SOHO) satellite showed that in the core of a quiescent equatorial streamer, oxygen was depleted by an order of magnitude compared with the photosphere, while it was depleted by a factor three at the streamer edge (Raymond et al. 1997). At least the streamer core measurements stem from altitudes where coronal gravitational settling can be significant, and it is not clear how much of the observed depletions, if any, reflect a depletion in the upper chromosphere.

Our models always started from a well mixed chromosphere with constant abundances. Presumably, the plasma of the closed field coronal structures must be the result of many such evaporation events. (The open field regions may be different, as the solar wind flow pulls matter through these regions.) Without an external process that reestablishes near photospheric abundances in the chromosphere, the upper chromosphere could then become progressively more depleted in high-FIP elements in particular, in turn causing the corona to become more depleted in these elements. The question is open whether the chromospheric mixing—which must take place, otherwise we would not observe high-FIP elements such as oxygen in the corona—is a separate process from the evaporation process. If the evaporation is caused by an increase in the coronal heating rate, as discussed above, then the "refilling" of the chromosphere after the event is probably caused by coronal and transition region matter cooling and recombining to form the new upper chromosphere. In that case, another process is probably required to remix the chromosphere below the evaporation region. To address these issues, a more comprehensive model is required, spanning the chromosphere, transition region, and corona.

Most of the observational papers report relative abundance enhancements (see introduction) and the mechanism discussed here can account for such enhancements, with the qualifications discussed above. However, absolute enhancement of iron relative to H has also been reported (White et al. 2000). As pointed out above, the mechanism presented here is not able to account for absolute enhancements that might exist at least in some observed coronal structures. On the other hand, we have shown that the balance between Coulomb collisions and gravitational settling plays a significant role in determining the abundances of the elements, and a theory that is developed to explain absolute enhancements of the low-FIP elements must account for the mechanism discussed here. Since observations of relative enhancements of low-FIP elements can be explained by the gravitational settling process, while absolute enhancements (relative to hydrogen) can not and would require other mechanisms, such as the Alfvén wave ponderomotive force studied by Laming (2004), more observations of absolute abundances would be particularly valuable in clarifying these mechanisms.

We thank the Institute of Theoretical Astrophysics at the University of Oslo, Norway, for their support. One of us (R.E.) thanks Mike Bird and the Argelander-Institute for Astronomy at the University of Bonn, Germany, for their hospitality.

REFERENCES

Arnaud, M., & Raymond, J. 1992, ApJ, 398, 394
Arnaud, M., & Rothenflug, R. 1985, A&AS, 60, 425
Bahcall, J. N., Basu, S., & Serenelli, A. M. 2005, ApJ, 631, 1281
Drake, J. J., & Testa, P. 2005, Natur, 436, 525
Dwivedi, B. N., Curdt, W., & Wilhelm, K. 1999, in ESA Special Publication, Vol. 446, 8th SOHO Workshop: Plasma Dynamics and Diagnostics in the Solar Transition Region and Corona, ed. J.-C. Vial & B. Kaldeich-Schü (Dordrecht: Kluwer), 293
Feldman, U., Schühle, U., Widing, K. G., & Laming, J. M. 1998, ApJ, 505, 999
Feldman, U., & Widing, K. G. 2003, SSRv, 107, 665
Fontenla, J. M., Avrett, E. H., & Loeser, R. 1990, ApJ, 355, 700
Gloeckler, G., & Geiss, J. 2007, SSRv, 130, 139
Hansteen, V. H., & Leer, E. 1995, JGR, 100, 21577
Hénoux, J.-C. 1998, SSRv, 85, 215
Killie, M. A., & Lie-Svendsen, Ø. 2007, ApJ, 666, 501
Korevaar, P., & van Leer, B. 1988, A&A, 200, 153
Laming, J. M. 2004, ApJ, 614, 1063
Landini, M., & Monsignori Fossi, B. C. 1975, A&A, 42, 213
Lepri, S. T., Zurbuchen, T. H., Fisk, L. A., et al. 2001, JGR, 106, 29231

Marsch, E., von Steiger, R., & Bochsler, P. 1995, A&A, 301, 261
Nakada, M. P. 1969, SoPh, 7, 303
Pucci, S., Lie-Svendsen, Ø., & Esser, R. 2010, ApJ, 709, 993
Raymond, J. C. 1999, SSRv, 87, 55
Raymond, J. C., Kohl, J. L., Noci, G., et al. 1997, SoPh, 175, 645
Rosner, R., Tucker, W. H., & Vaiana, G. S. 1978, ApJ, 220, 643
Schultz, D. R., Krstic, P. S., Lee, T. G., & Raymond, J. C. 2008, ApJ, 678, 950
Schunk, R. W. 1977, RvGSP, 15, 429
Vauclair, S. 1996, A&A, 308, 228
Vernazza, J. E., Avrett, E. H., & Loeser, R. 1981, ApJS, 45, 635
von Steiger, R., & Geiss, J. 1989, A&A, 225, 222
von Steiger, R., Schwadron, N. A., Fisk, L. A., et al. 2000, JGR, 105, 27217
Wang, Y.-M. 1996, ApJL, 464, L91
White, S. M., Thomas, R. J., Brosius, J. W., & Kundu, M. R. 2000, ApJL, 534, L203
Widing, K. G., & Feldman, U. 2001, ApJ, 555, 426